Increasing the conformational stability by replacement of heme axial ligand in *c*-type cytochrome

Tadashi Satoh[a], Akito Itoga[a], Yasuhiro Isogai[b], Masaaki Kurihara[c], Seiji Yamada[a], Miwa Natori[a], Noriko Suzuki[a], Kohei Suruga[a], Ryu Kawachi[a], Masaomi Arahira[d], Toshiyuki Nishio[a], Chikafusa Fukazawa[d], Tadatake Oku[a,*]

[a] *Department of Biological Chemistry, College of Bioresource Sciences, Nihon University, Kameino 1866, Fujisawa, Kanagawa 252-8510, Japan*
[b] *RIKEN, Hirosawa 2-1, Wako, Saitama 351-0198, Japan*
[c] *National Institute of Health Sciences, Kamiyoga 1-18-1, Setagaya, Tokyo 158-8501, Japan*
[d] *Genetic Engineering Laboratory, National Food Research Institute, Tsukuba, Ibaraki 305-8642, Japan*

Received 23 August 2002; accepted 2 October 2002

First published online 29 October 2002

Edited by Richard Cogdell

Abstract To investigate the role of the heme axial ligand in the conformational stability of *c*-type cytochrome, we constructed M58C and M58H mutants of the red alga *Porphyra yezoensis* cytochrome c_6 in which the sixth heme iron ligand (Met58) was replaced with Cys and His residues, respectively. The Gibbs free energy change for unfolding of the M58H mutant in water ($\Delta G°_{unf}$ = 1.48 kcal/mol) was lower than that of the wild-type (2.43 kcal/mol), possibly due to the steric effects of the mutation on the apoprotein structure. On the other hand, the M58C mutant exhibited a $\Delta G°_{unf}$ of 5.45 kcal/mol, a significant increase by 3.02 kcal/mol compared with that of wild-type. This increase was possibly responsible for the sixth heme axial bond of M58C mutant being more stable than that of wild-type according to the heme-bound denaturation curve. Based on these observations, we propose that the sixth heme axial ligand is an important key to determine the conformational stability of *c*-type cytochromes, and the sixth Cys heme ligand will give stabilizing effects.

Key words: Axial ligand; Conformational stability; Cytochrome c_6; Heme iron; *Porphyra yezoensis*

1. Introduction

Heme proteins exhibit an extensive array of biological functions including electron carrier as cytochrome *c*, enzymes as catalase, and oxygen storage/transport proteins as myoglobins and hemoglobins. The functions of the heme proteins can be attributed to the diversity of the protein structure, the heme prosthetic group (e.g. heme *a*, heme *c*, protoheme, siroheme), and the fifth and sixth heme axial ligands. In the case of *c*-type cytochromes, the protoheme is covalently bonded via thioether linkages to the two Cys residues, and the axial His and Met ligands are generally coordinated to the heme iron as its fifth and sixth ligands, respectively [1–3]. On the other hand, the *b*-type heme proteins (e.g. peroxidases [4], myoglobin [5]) have a fifth His ligand and a sixth H_2O ligand, and many *b*-type cytochromes [6] have bis-His ligands. Furthermore, cytochrome P450 [7] has a fifth Cys ligand and a sixth H_2O ligand. Thus, heme proteins have various axial ligation patterns, and the ligands play essential roles in the functions of heme proteins [2–7]. For example, in horse heart cytochrome *c*, the replacement of axial Met80 with Cys caused a significant decrease in the redox potential from 262 mV to −390 mV [2].

Studies on improving the conformational stability of general non-heme proteins have been extensively conducted by site-directed mutagenesis [8–12]. According to those studies, examples of strategies for increasing the stability are as follows: increase in internal hydrophobicity [8], introduction of hydrogen bonds and salt bridges [9,10], introduction of a disulfide bond [11], and replacement with Pro [12]. On the other hand, the relationship between the stability of heme proteins and the axial ligands remains to be clarified [13].

In our laboratory, the structure/function relationships of cytochromes *c* have been investigated [14–16]. In the case of the red alga *Porphyra yezoensis* cytochrome c_6 [15], we have determined its primary and tertiary structures (JC5849 (PIR number), AB040818 (DDBJ number) and 1gdv (PDB code)), and investigated the correlation between the structure and the redox potential, which was the highest (370 mV) among soluble heme proteins. Cytochrome c_6 is a class I *c*-type cytochrome, in which the heme iron has Met-His axial coordination, and functions as an electron carrier between cytochrome b_6f and the P700 reaction center of photosystem I in the thylakoid lumen. In this work, we investigated the role of heme axial ligands in the conformational stability of cytochrome c_6 from *P. yezoensis* by site-directed mutagenesis studies.

2. Materials and methods

2.1. Construction of expression vectors

Construction and overproduction of the cytochrome c_6 gene (*pet*J) in *Escherichia coli* were performed according to a method described by Arslan et al. [17] with slight modifications. The matured *pet*J sequence was amplified using the forward primer P1: 5′-GCAGATCTAGATAATGGAGAAAAAG-3′ corresponding to codons for amino acid residues 1–9 of the cytochrome c_6 N-terminal region, and the

*Corresponding author. Fax: (81)-466-84 3950.
E-mail address: oku@brs.nihon-u.ac.jp (T. Oku).

Abbreviations: CD, circular dichroism; E_m, midpoint redox potential; non-mutant, recombinant protein without any mutation; PCR, polymerase chain reaction

0014-5793/02/$22.00 © 2002 Published by Elsevier Science B.V. on behalf of the Federation of European Biochemical Societies.
PII: S0014-5793(02)03615-3

reverse primer P2: 5′-GCGGATCCTTACCAACCTTTTTCAGATTGAG-3′ corresponding to the C-terminal region. The amplified *pet*J sequence was ligated to the *pel*B signal sequence adapter (synthesized by Sawady Technology Co.). The resulting *pel*B–*pet*J hybrid gene was cloned into *Nde*I–*Bam*HI sites of pET22b(+) (Novagen) to create the plasmid pET22*Pyc*$_6$.

Cytochrome *c* maturation genes, *ccmA–H*, were polymerase chain reaction (PCR)-amplified from *E. coli* MC1061 genomic DNA using the forward primer P3: 5′-CCAGAATTCGGTTGCCGCGAAGATGCAT-3′ corresponding to upstream of the *ccm*A gene from the *E. coli* K12 MG1655 genome sequence (AE000309), and the reverse primer P4: 5′-TTCCTGCAGCAACGCGGGGCACAATAAA-3′ corresponding to downstream of the *ccm*H gene. The resulting *ccmA–H* gene was cloned into *Eco*I–*Pst*I sites of pSTV28 (Takara Shuzo Co.) to create the plasmid pSTV28*ccmA–H*.

2.2. Site-directed mutagenesis

The mutations of *pet*J were introduced by the megaprimer PCR method [18]. The mutagenic oligonucleotides P5: 5′-GGTAAAAATGCCTGCCCTGCTTTCGGAGG-3′ and P6: 5′-GGTAAAAATGCCCATCCTGCTTTCGGAGG-3′ were used to change the ATG codon encoding Met58 into TGC (Cys) and CAT (His), respectively.

2.3. Protein expression and purification

Purification of wild-type cytochrome c_6 was performed as previously described [15]. For the overproduction of mutant cytochrome c_6, both pET22*Pyc*$_6$(mutant) and pSTV28*ccmA–H* were co-introduced into *E. coli* BL21(DE3). The procedure for the overproduction of cytochrome c_6 followed that described previously [19] with slight modifications. The synthesized mutants were purified by BioCAD700E perfusion chromatography (Applied Biosystems) according to the method for the wild-type. The degree of purity was confirmed from the absorbance ratio A_{275}/A_{553} and tricine–SDS–PAGE [20].

2.4. Spectroscopic analysis

UV/visible spectra were measured with a Hitachi U3310 spectrophotometer using quartz cuvettes of 1.0 cm path length. Protein concentrations of cytochromes c_6 were determined spectrophotometrically from the pyridine ferrohemochrome spectrum (550 nm, 29.1 mM^{-1} cm^{-1}) [21]. Circular dichroism (CD) spectra were recorded at 25°C in 20 mM sodium phosphate buffer (pH 7.0) with a Jasco J720 spectropolarimeter using 0.2 cm path length rectangular quartz cuvettes. The α-helical contents were calculated from the CD absorbance at 222 nm based on the 100% value of −32 000 deg cm^2/dmol [22].

2.5. Redox titrations

Redox titrations were performed under anaerobic conditions with a continuous stream of argon, in 100 mM sodium phosphate buffer (pH 7.0) at 25°C [23]. The potentials were measured with a Horiba F-13 pH meter equipped with an ORP electrode, and the optical spectra were recorded throughout the titration on a Hitachi U3310 spectrophotometer. The redox mediators were used to stabilize the solution redox potential as described previously [14] except for the measurement of the M58C mutant. For the M58C mutant, the following mediators were used: 20 μM duroquinone, 10 μM 2-hydroxy-1,4-naphthoquinone, 10 μM anthraquinone-2-sulfonate, 2 μM benzyl viologen, 1 μM phenylsafranine, and 1 μM indigo carmine. The redox data were analyzed from the theoretical curve obtained using the Nernst equation ($n = 0.9$–1.1): $E = E^0 + (RT/nF)$ ln ([ferric]/[ferrous]).

2.6. Denaturation

Quantitative disruption of protein structures with guanidine hydrochloride (Gdn-HCl) as denaturant was measured by monitoring the CD signal intensity at 222 nm or by monitoring the Soret absorbance peaks of heme-bound proteins as a function of Gdn-HCl concentration. The protein solutions (5 μM protein in 10 mM sodium phosphate (pH 7.0) containing Gdn-HCl) were incubated for 1 day at 4°C to reach equilibrium, and the CD and visible spectra were measured at 25°C. The denaturation data were analyzed with a theoretical curve based on $\Delta G_{unf} = -RT\ln K_D = \Delta G°_{unf} - m[\text{Gdn-HCl}]$ by assuming the two-state folding–unfolding transition with the equilibrium constant K_D [24]. The thermodynamic parameter, $\Delta G°_{unf}$, shows free energy change from the folded state to the unfolded state in the absence of a denaturant, and m shows the dependence of the free energy change ($\Delta G°_{unf}$) on the denaturant concentration. Thermal denaturation of the proteins was measured by monitoring the CD signal intensity at 222 nm as a function of temperature (40°C/h from 5 to 95°C), and the data were fit to a two-state model [25] to yield T_m.

2.7. Computational procedure

The initial structures of the molecules were constructed using (MacroModel) with the crystal structure of *P. yezoensis* cytochrome c_6 (1gdv). Geometry optimization and computation of the electronic structures of the molecules were conducted by ab initio molecular orbital calculation (UHF: STO-3G level), using *SPARTAN*. All computations were conducted on an SGI workstation.

3. Results and discussion

3.1. Construction and overproduction of mutant cytochromes c_6

To investigate the role of the axial ligands in the conformational stability of *P. yezoensis* cytochrome c_6, we constructed the M58C and M58H mutants of cytochrome c_6 in which the sixth heme iron ligand (Met58) was replaced with Cys and His, respectively; those amino acid residues are the axial ligands in many natural heme proteins, and were selected as the sixth heme axial ligand instead of Met58 in the cytochrome c_6. *E. coli* BL21(DE3) cells harboring both pET22*Pyc*$_6$(mutant) and pSTV28*ccmA–H* were able to overproduce recombinant cytochromes c_6. The recombinant protein without any mutations is designated non-mutant. The cell pellets were reddish brown, indicating heme protein overproduction. About 2 mg of recombinant cytochromes c_6 was obtained from a 1 l culture of *E. coli* cells cotransformed with the *ccmA–H* gene cluster. Each of the recombinant cytochromes c_6 was effectively transported to the periplasm of *E. coli* using the *pel*B signal sequence, and the sequence was cleaved off by signal peptidase, as deduced from the N-terminal amino acid sequence.

3.2. UV/visible spectra and redox potential of the mutant cytochromes c_6

As shown in Fig. 1, the UV/visible absorption spectra of the non-mutant were quite similar to those of wild-type cytochrome c_6. The ferric forms showed visible absorption maxima at 526 (α+β) and 409 (Soret) nm, and the ferrous forms at 553 (α), 522 (β), and 416 (Soret) nm. The absorption peaks for the ferric and ferrous forms were assigned to the low-spin Met-His axial coordinated heme iron, which is characterized by class I *c*-type cytochromes [1]. Moreover, the midpoint redox potential (E_m) of the non-mutant (370 mV) was almost identical to that of the wild-type (371 mV). For the M58C mutant, the ferric forms showed absorption peaks at 566, 539 (α+β) and 418 (Soret) nm, and the ferrous forms at 553 (α), 522 (β), and 417 (Soret) nm (Fig. 1C). In addition, the E_m of the M58C mutant (−286 mV) showed a significant decrease of −657 mV compared with that of the wild-type (371 mV). These results are generally consistent with the absorption peak and the E_m of cytochrome *c*-Cys80 [2], indicating that the sixth ligand of the heme iron of the M58C mutant was Cys. On the other hand, the ferric forms of the M58H mutant showed absorption peaks at 529 (α+β) and 408 (Soret) nm, and the ferrous forms at 554 (α), 523 (β), and 417 (Soret) nm (Fig. 1D). Furthermore, the absorption peak at 695 nm, which is observed in sulfur (Met) charge transfer to Fe^{3+}, disappeared in the ferric form of the M58H. The E_m of the M58H mutant (82 mV) was lower than that of the wild-type (371 mV), and this phenomenon agrees with that of cytochrome *c*-His80 [3]. From these results, we conclude that the

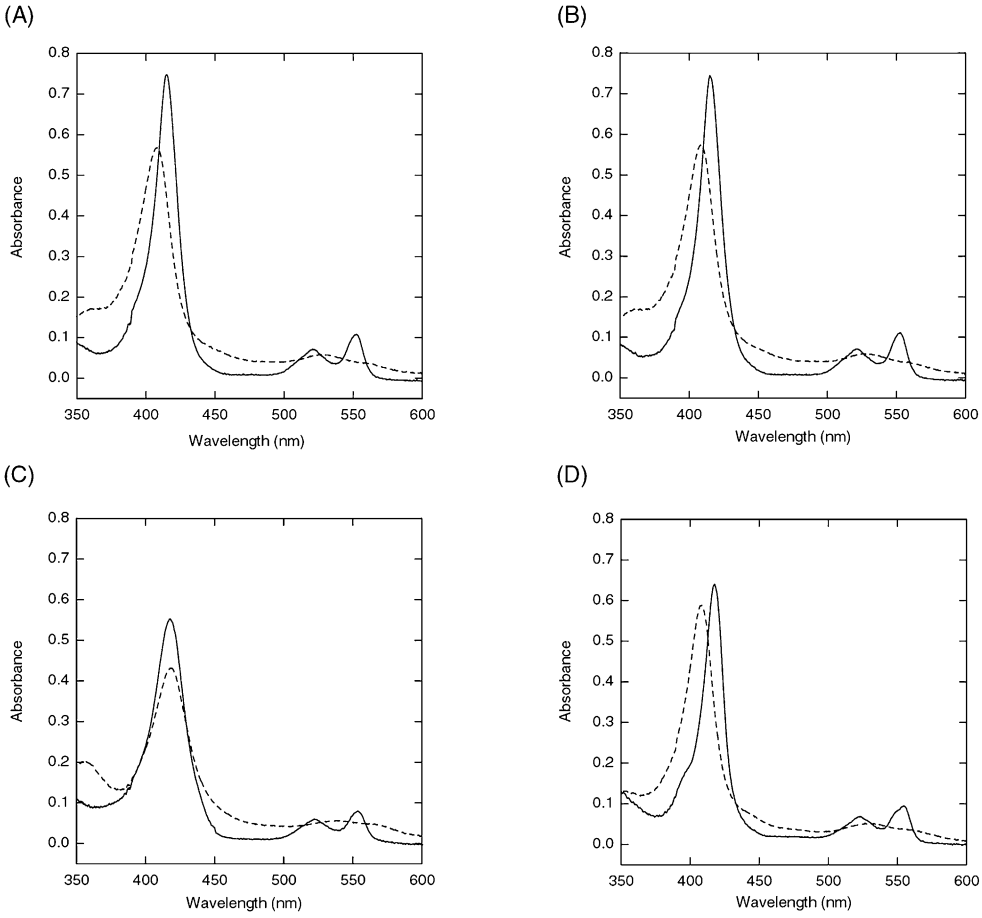

Fig. 1. UV/visible spectra of the ferrous and ferric forms of wild-type and mutant cytochromes c_6. Absorption spectra of 5 μM cytochrome c_6 were measured in 10 mM sodium phosphate (pH 7.0) at 25°C. A: Wild-type; B: non-mutant; C: M58C; D: M58H.

sixth ligand of the heme iron of the M58H mutant was His. The pyridine ferrohemo-chromogens of these cytochromes c_6 had an α-band at 550 nm, indicating that their prosthetic groups were heme *c* [21].

3.3. Secondary structure of the mutant cytochromes c_6

The helical nature of the recombinant cytochromes c_6 was confirmed by far-UV CD measurement, which is able to probe the secondary structure of globular proteins (Fig. 2). The α-helical contents of the wild-type, non-mutant, M58C and M58H cytochromes c_6 under the experimental conditions (20 mM sodium phosphate (pH 7.0) at 25°C) were estimated to be 72.7, 73.8, 74.6 and 66.1%, respectively, based on the ellipticity of −32 000 deg cm^2/dmol for 100% helicity [22]. Accordingly, the non-mutant and the M58C mutant preserved their α-helical contents to almost the same degree as that of the wild-type cytochrome c_6. On the other hand, the α-helical content of the M58H was slightly less than that of wild-type cytochrome c_6, and this may be due to the perturbation of the short β-sheet structure (residues 55–58) [15] by the replacement of Met58 with His58, which has a low tendency to form the β-sheet structure [26].

3.4. Role of the heme axial ligand in conformational stability of cytochrome c_6

The denaturation of the cytochromes c_6 mutants with GdnHCl was measured by monitoring the CD signal intensity at 222 nm or by monitoring the Soret absorbance peaks (Fig. 3). The denaturation curve of the non-mutant, which was obtained by monitoring the α-helix structure ($C_m = 0.95$ M), was quite similar to that of wild-type cytochrome c_6 ($C_m = 0.95$ M) (Table 1). Thermodynamic parameters of the cytochromes c_6 mutants, which were obtained by assuming a simple two-state folding–unfolding transition, are summarized

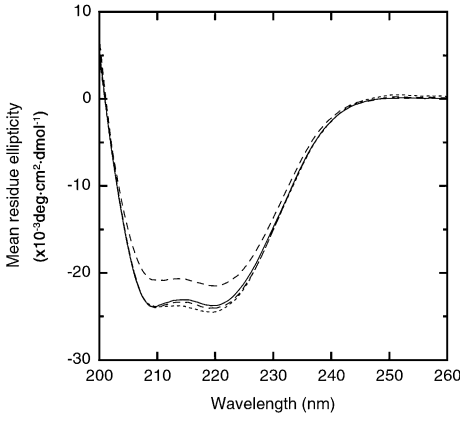

Fig. 2. CD spectra of wild-type cytochrome c_6 (solid line), non-mutant (dotted line), M58C (dashed line) and M58H (semi-dotted line). The spectra were recorded in 10 mM sodium phosphate (pH 7.0) at 25°C. The protein concentrations were 10 μM as determined spectrophotometrically.

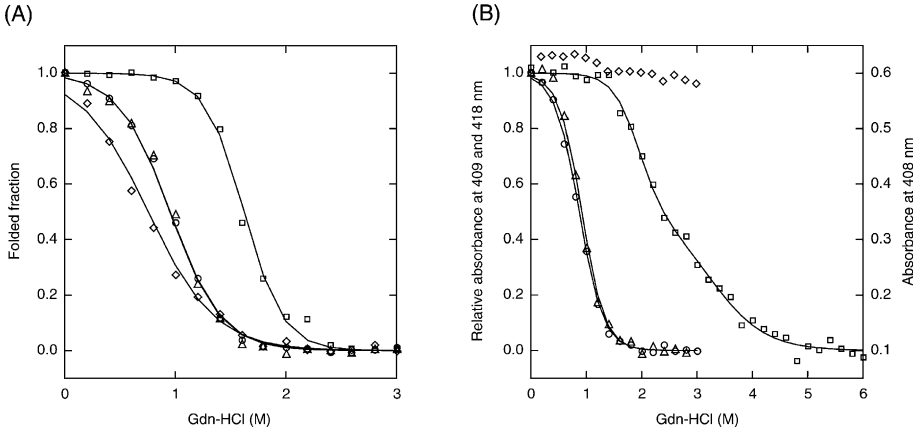

Fig. 3. Denaturation curves of wild-type and mutant cytochromes c_6. The secondary structures of wild-type and mutant cytochromes c_6 were monitored from the CD signal intensity at 222 nm against Gdn-HCl concentration at 25°C (A). The dissociation of heme in wild-type, non-mutant, M58C and M58H cytochromes c_6 was monitored from the Soret absorption peaks at 409, 409, 418 and 408 nm, respectively (B). The proteins were denatured by titration with Gdn-HCl in 10 mM sodium phosphate (pH 7.0) at a protein concentration of 5 μM. Wild-type (circles); non-mutant (triangles); M58C (squares); M58H (diamonds).

in Table 1. Furthermore, the α-helical denaturation curves of the wild-type and the non-mutant were quite similar to their respective heme-bound denaturation curves (Fig. 3B), indicating that the dissociation of the sixth Met ligand is tightly coupled with the unfolding of cytochrome c_6. This agrees with the protein unfolding of horse heart cytochrome *c* [27].

The $\Delta G°_{unf}$ of 1.48 kcal/mol and the *m* of 1.96 kcal/mol/M of the M58H mutant were smaller than those of the wild-type (2.43 kcal/mol and 2.56 kcal/mol/M, respectively), as shown in Table 1. The decrease in the thermodynamic stability of M58H is attributable to the perturbation of the secondary structure (Fig. 2). In contrast, the axial coordination with His58 was significantly strong and was almost unchanged during the Gdn-HCl denaturation (Fig. 3B). Therefore, in contrast with the native cytochrome, the unfolding of the M58H mutant is independent of the dissociation of the sixth His ligand.

On the other hand, the $\Delta G°_{unf}$ and *m* values of the M58C mutant were 5.45 kcal/mol and 3.36 kcal/mol/M, respectively, and a significant increase of 3.02 kcal/mol in the conformational stability ($\Delta G°_{unf}$) was realized compared with the wild-type. Furthermore, the axial bond of Fe^{3+}–Cys was more stable than Fe^{3+}–Met in the proteins according to the heme-bound denaturation curve (Fig. 3B). However, the denaturation curve of M58C was fairly dissimilar to that obtained by monitoring the CD signals. The heme-bound denaturation occurred apparently via three-state transitions (folded state (F) ⇔ intermediate (I) ⇔ unfolded state (U)). The former transition (F ⇔ I) occurred in the same Gdn-HCl concentration range (0–2.2 M) as the protein unfolds, whereas the latter transition (I ⇔ U) occurred at higher concentrations of the denaturant (over 2.2 M) (Fig. 3). The former transition seems to correspond to the dissociation of the Fe^{3+}–Cys bond, indicating that the dissociation couples with the protein unfolding. Thus, the increase in $\Delta G°_{unf}$ (3.02 kcal/mol) of the α-helical structure of the M58C mutant is possibly due to the enhancement of the axial bond strength.

Ab initio energy calculation shows that the bonds of N(His)–Fe^{3+} and S(Cys)–Fe^{3+} are more stable than that of S(Met)–Fe^{3+} by 5.2 and 17.8 kcal/mol, respectively. These values cannot be simply compared with the experimental data obtained here (Fig. 3B) because the measured $\Delta G°_{unf}$ values are different between the folded and unfolded states and the energies of each unfolded state are not involved in the calculated values. However, the theoretical data suggest the bonds energies of N(His)–Fe^{3+} and S(Cys)–Fe^{3+} are significantly higher than that of S(Met)–Fe^{3+} and consistent with the experimental results (Fig. 3B).

The effects of the ligand exchanges between M58H and M58C mutants are contrastive. Although the axial bond of the Fe^{3+}–His is stronger than that of Fe^{3+}–Met (Fig. 3B), the replacement with His decreases the stability. The ligand change from Met to His gives destabilizing effects in the protein structure, e.g. exposure of the hydrophobic residues to the solvent, which agrees with the decrease of the α-helical contents (Fig. 2). This structural change may dissect the heme dissociation reaction from the protein unfolding (Fig. 3). On the other hand, the ligand change from Met to Cys gives stabilizing effects through the formation of a stable bond between the ligand and the heme iron, which is consistent with

Table 1
Thermal and Gdn-HCl denaturation data

Cytochrome	C_m (M)[a]	$\Delta G°_{unf}$ (kcal/mol)[b]	*m* (kcal/mol/M)[c]	T_m (°C)[d]
Wild-type	0.95	2.43	2.56	48.83
Non-mutant	0.95	2.42	2.54	49.57
M58C	1.62	5.45	3.36	58.45
M58H	0.76	1.48	1.96	48.73

[a]Midpoint of the unfolding transition determined by Gdn-HCl denaturation.
[b]Free energy change (ΔG_{unf}) from the folded state to the unfolded state in the absence of denaturant.
[c]Dependence of free energy change (ΔG_{unf}) on Gdn-HCl concentration.
[d]Midpoint of the thermal denaturation transition.

the native protein structure and preserves the coupling between the heme binding and the protein folding. This agrees with the result that the secondary structure was not affected by the mutation in the absence of Gdn-HCl (Fig. 2).

In conclusion, we propose that the sixth heme axial ligand is an important key to determine thermodynamic stability of *c*-type cytochromes, and the sixth Cys heme ligand will give stabilizing effects owing to the formation of stable axial bond between the heme iron and the sixth ligand.

Acknowledgements: We are indebted to Mr. Hayato Yamaya and Ms. Natsuki Tsumoto of Nihon University for the purification of cytochrome c_6 mutants from *E. coli*. This work was supported in part by a Grant-in-Aid for Research for the Future Program (JSPS-RFTF97R16001) from the Japan Society for the Promotion of Science and for Scientific Research (C) from the Ministry of Education, Culture, Sports, Science, and Technology of Japan (2001).

References

[1] Pettigrew, G.W. and Moore, G.R. (1990) Cytochromes *c*: Evolutionary, Structural and Physicochemical Aspects, pp. 161–170, Springer, Berlin.
[2] Rapael, A.L. and Gray, H.B. (1991) J. Am. Chem. Soc. 113, 1038–1040.
[3] Wallace, C.J.A. and Clark-Lewis, I. (1992) J. Biol. Chem. 267, 3852–3861.
[4] Hirst, J., Wilcox, S.K., Ai, J., Moënne-Loccoz, P., Loehr, T.M. and Goodin, D.B. (2001) Biochemistry 40, 1274–1283.
[5] Adachi, S., Nagano, S., Ishimori, K., Watanabe, Y. and Morishima, I. (1993) Biochemistry 32, 241–252.
[6] Mowat, C.G., Miles, C.S., Munro, A.W., Cheesman, M.R., Quaroni, L.G., Reid, G.A. and Chapman, S.K. (2000) J. Biol. Inorg. Chem. 5, 584–592.
[7] Auclair, K., Moënne-Loccoz, P. and Ortiz de Montellano, P.R. (2001) J. Am. Chem. Soc. 123, 4877–4885.
[8] Yutani, K., Ogasawara, K., Tsujita, T. and Sugino, Y. (1987) Proc. Natl. Acad. Sci. USA 84, 4441–4444.
[9] Alber, T., Dao-Pin, S., Wilson, K., Wozniak, J.A., Cook, S.P. and Matthews, B.W. (1987) Nature 330, 41–46.
[10] Spek, E.J., Bui, A.H., Lu, M. and Kallenbach, N.R. (1998) Protein Sci. 7, 2431–2437.
[11] Kurioki, K., Inaka, K., Taniyama, Y., Kidokoro, S., Matsushima, M., Kikuchi, M. and Yutani, K. (1992) Biochemistry 31, 8323–8328.
[12] Herning, T., Yutani, K., Inaka, K., Kuroki, R., Matsushima, M. and Kikuchi, M. (1992) Biochemistry 31, 7077–7085.
[13] Hargrove, M.S. and Olson, J.S. (1996) Biochemistry 35, 11310–11318.
[14] Yamada, S., Nakamura, T., Tanaka, Y., Isogai, Y., Nishio, T. and Oku, T. (2000) Biosci. Biotechnol. Biochem. 64, 628–632.
[15] Yamada, S., Park, S.-Y., Shimizu, H., Koshizuka, Y., Kadokura, K., Satoh, T., Suruga, K., Ogawa, M., Isogai, Y., Nishio, T., Shiro, Y. and Oku, T. (2000) Acta Crystallogr. D56, 1577–1582.
[16] Yamada, S., Suruga, K., Ogawa, M., Hama, T., Satoh, T., Kawachi, R., Nishio, T. and Oku, T. (2002) Biosci. Biotechnol. Biochem. 66, 2044–2051.
[17] Arslan, E., Schulz, H., Zufferey, R., Künzler, P. and Thöny-Meyer, L. (1998) Biochem. Biophys. Res. Commun. 251, 744–747.
[18] Sambrook, J. and Russell, D.W. (2001) Molecular Cloning. A Laboratory Manual, 3rd edn., pp. 1331–1335, Cold Spring Harbor Laboratory Press, Cold Spring Harbor, NY.
[19] Sanders, C. and Lill, H. (2000) Biochim. Biophys. Acta 1459, 131–138.
[20] Schägger, H. and Jagow, G.V. (1987) Anal. Biochem. 166, 368–379.
[21] Drabkin, D.L. (1942) J. Biol. Chem. 146, 605–617.
[22] Pace, C.N., Shirly, B.A. and Thompson, J.A. (1989) Protein Structure: A Practical Approach, pp. 311–330, IRL, Oxford.
[23] Dutton, P.L. (1978) Methods Enzymol. 54, 411–435.
[24] Pace, C.N. (1986) Methods Enzymol. 131, 266–280.
[25] Allen, D.L. and Pielak, G.J. (1998) Protein Sci. 7, 1262–1263.
[26] Chou, P.Y. and Fasman, G.D. (1978) Adv. Enzymol. 47, 45–148.
[27] Yeh, S-R. and Rousseau, D.L. (1999) J. Biol. Chem. 274, 17853–17859.